Progress in Microbes and Molecular Biology

HH PUBLISHER

Original Research Article

Brain-Eating Amoeba Meets Plant Defense: *In Vitro* and *In Silico* Evaluation of Malabaricones as Potent Anti-*Naegleria fowleri* Agents

Kavitha Rajendran[1*], Lemmuel Tayo[2,3*], Marineil Gomez[3,4], Devandran Apparasamy[1], Haema Thevanayagam[5], Shealtiel William Chan[2,3], Ryan Christian Mailem[2,3], Regine Menente[2], Catherine Joyce Rueda[2], Yasodha Sivasothy[6], Muhamad Aqmal Othman[7], Usman Ahmed[8], Niwasini Krishna Kumar[1], Chris Izaak Jones[8], Ayaz Anwar[8]

Article History

Received: 22 May 2025;

Received in Revised Form: 11 August 2025;

Accepted: 13 August 2025;

Available Online: 29 August 2025

[1]School of American Education (SAE), Sunway University, Subang Jaya, Selangor 47500, Malaysia; devana@sunway.edu.my (DA); niwasini17@hotmail.com (NKK)

[2]School of Health Sciences, Mapua University, Makati City, Metro Manila 1205, Philippines; swschan@mapua.edu.ph (SWC); rcmailem@mapua.edu.ph (RCM); rgmenente@mymail.mapua.edu.ph (RM); jcprueda@mymail.mapua.edu.ph (CR)

[3]School of Chemical, Biological and Materials Engineering and Sciences, Mapua University, Makati City, Metro Manila 1002, Philippines

[4]School of Graduate Studies, Mapua University, Makati City, Metro Manila 102, Philippines; mcgomez@mapua.edu.ph (MG)

[5]Department of Science and Engineering Resources, Sunway University, Subang Jaya, Selangor 47500, Malaysia; haemat@sunway.edu.my (HT)

[6]School Pharmacy, Monash University Malaysia, Subang Jaya, Selangor 47500, Malaysia; yasodhasivasothy@gmail.com (YS)

[7]Department of Chemistry, University Malaya, Kuala Lumpur, Selangor 50603, Malaysia; aqmal@um.edu.my (MAO)

[8]Department of Biological Sciences, Sunway University, Subang Jaya, Selangor 47500, Malaysia; 19094465@imail.sunway.edu.my (UA); 24121543@imail.sunway.edu.my (CIJ); ayazanwarkk@yahoo.com (AA)

*Corresponding author: Kavitha Rajendran; School of American Education (SAE), Sunway University, 47500 Selangor, Malaysia; kavithar@sunway.edu.my (KR); Lemmuel Tayo; School of Health Sciences, Mapua University, Makati City, Metro Manila 1205, Philippines, lltayo@mapua.edu.ph (LT)

Abstract: *Naegleria fowleri (N. fowleri)* is a thermophilic, free-living amoeba that causes primary amoebic meningoencephalitis (PAM), a rapidly fatal brain infection with a mortality rate exceeding 97%. Current treatments are limited and often ineffective, creating an urgent need for new anti-amoebic agents. This study investigates, for the first time, the anti-amoebic potential of malabaricone A-C acylphenol compounds isolated from *Myristica cinnamomea* (cinnamon nutmeg) against *N. fowleri*, using both *in vitro* and *in silico* approaches. Parasite

viability assays were conducted to evaluate the amoebicidal activity of each compound, while cytotoxicity tests on human cell lines assessed their selectivity. Molecular docking studies were performed to predict binding affinities to *N. fowleri* therapeutic targets, and ADMET profiling evaluated drug-likeness and toxicity. All three malabaricones significantly reduced trophozoite viability, with malabaricone B showing the greatest potency, followed by malabaricone C. Treated amoebae exhibited disrupted membranes, consistent with cell death. Importantly, all compounds displayed low cytotoxicity to mammalian cells at effective concentrations. *In silico* docking revealed strong binding affinities of the malabaricones, particularly malabaricone B, toward key amoebic proteins involved in metabolism and cell regulation. ADMET predictions indicated favourable pharmacokinetic and safety profiles. This study demonstrates that malabaricone A–C, especially malabaricone B, exhibit potent and selective anti-amoebic activity against *N. fowleri*, supported by both experimental and computational analyses. These findings position malabaricones as promising natural lead compounds for developing new PAM therapies, addressing a critical unmet need in anti-amoebic drug discovery. By identifying novel natural leads against a neglected yet deadly infection, this study advances Sustainable Development Goal 3 by promoting safer, more effective treatments and addressing health inequities in infectious disease care. Additionally, the integration of *in silico* methodologies aligns with Sustainable Development Goal 12 by fostering responsible consumption and production through the efficient use of natural resources and the reduction of experimental waste in drug discovery.

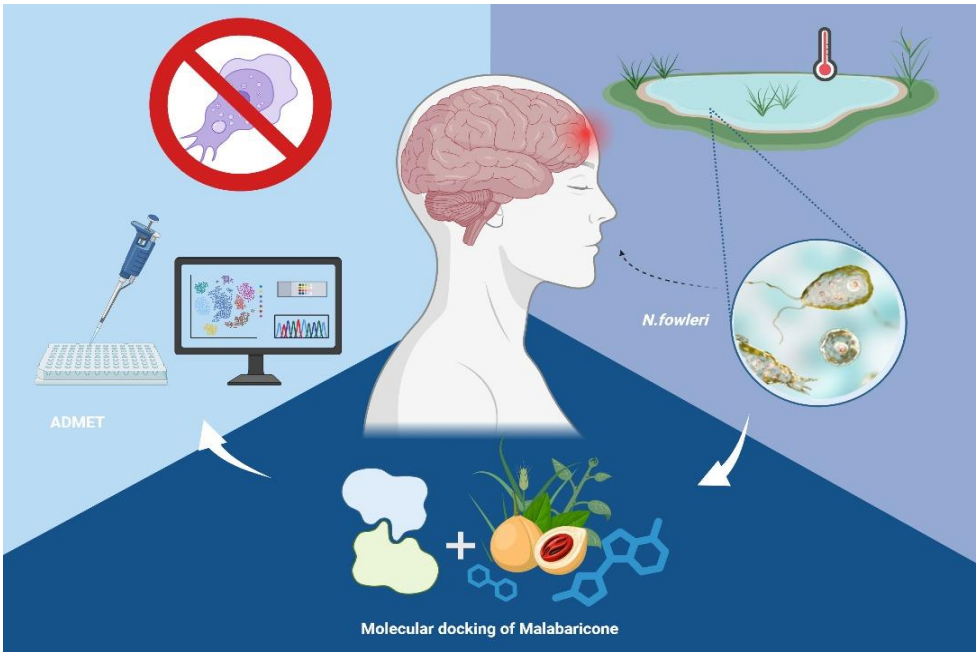

Graphical abstract. Overview of *in vitro* and *in silico* studies demonstrating the anti-amoebic effects of malabaricone against *N. fowleri.*

Keywords: *Naegleria fowleri*, Malabaricone, Anti-amoebic activity, Natural compound, Molecular Docking; SDG 3 Good health and well-being

1. Introduction

Naegleria fowleri (N. fowleri) is a free-living amoeba (a single-celled living organism) commonly found in warm lakes, rivers, hot springs in natural environments and in more rural area water heaters, tap water[1,2]. Among the various species of *Naegleria,* only one, *N. fowleri,* is known to infect humans. When water containing this pathogen enters the body through the nose, the amoeba travels up the nasal passages and into the brain, where it obliterates the brain tissue and causes primary amoebic meningoencephalitis (PAM), a fatal infection[3].This infection typically occurs when individuals engage in activities such as swimming, diving, or submerging their heads in freshwater environments like lakes and rivers. Although rare, infections can also result from exposure to recreational water sources such as pools, splash pads, or surf parks that are not adequately chlorinated. It is important to note that people cannot become infected with *N. fowleri* by drinking contaminated water[4]. *N. fowleri* exists in three distinct forms: a flagellate form that appears under non-nutritive conditions in the presence of water, a dormant cyst form that develops in extreme environmental conditions, and a metabolically active trophozoite stage that emerges under ideal conditions[5,6].The trophozoite is the only form capable of feeding, reproducing, and causing necrotising central nervous system (CNS) infections, which are characterised by significant brain oedema and neuronal damage resulting from cytotoxic molecules and inflammatory responses[7–9]. *N. fowleri* is a thermophilic, or heat-loving, organism. As such, it can grow at elevated temperatures up to 46°C and is capable of surviving for short periods at even higher temperatures[10]. Additionally, *N. fowleri* is not found in saltwater environments such as the ocean[10,11]. The infection caused by *N. fowleri* is not contagious; however, it carries an extremely high mortality rate due to the destruction of brain tissue, which leads to severe brain swelling and ultimately death. The fatality rate, 97% a critical factor in managing this infection is rapid diagnosis [8]. Identifying effective treatments has proven difficult, as the disease progresses swiftly. Currently, PAM is treated using a combination of drugs, most commonly including amphotericin B, azithromycin, fluconazole, rifampin, miltefosine, and dexamethasone[12]. These medications, however, must be administered in high concentrations, and many have limited ability to cross the blood-brain barrier (BBB) while also posing risks such as nephrotoxicity[5,13]. Given the aggressive nature of the infection and the limitations of current therapies, there is an urgent need for the development of safer and more effective treatments against *N. fowleri*[14]. Recent research has also explored investigational drugs like nitroxoline and the potential role of immunomodulatory agents in reducing neurological damage and improving outcomes[15].

In recent years, *in silico* techniques such as molecular docking has become indispensable in the early stages of drug discovery. These computational methods enable researchers to predict the binding affinity and orientation of small molecules within the active sites of target proteins, facilitating the identification of promising therapeutic candidates prior to in vitro testing[16]. This approach significantly reduces both the time and cost associated with traditional drug screening. Moreover, when molecular docking is combined with molecular dynamics simulations, it provides deeper insights into the stability, flexibility, and behavior of ligand-protein interactions under physiological conditions[17]. These integrated strategies have been successfully applied in parasitology and infectious disease research, including studies targeting *N. fowleri*, to identify novel inhibitors and optimize lead compounds[18].

Over the past several years, an extensive range of naturally occurring bioactive compounds such as essential oils have been systematically investigated for their anti-amoebic potential, with numerous studies reporting significant amoebicidal activity against *N. fowleri*[19–24]. In the present study, the malabaricone compounds derived from the fruit of cinnamon nutmeg were evaluated for the first time for their potential effectiveness against *N. fowleri*. Moreover, malabaricones have previously demonstrated antiparasitic activity, as evidenced by their ability to significantly inhibit trophozoite growth and impede encystation in *Acanthamoeba castellanii (A. castellani)*, while maintaining minimal cytotoxicity toward human cells, further supporting their potential as broad-spectrum anti-amoebic agents[25,26]. The genus *Myristica* is recognized for its rich phytochemical profile, encompassing a diverse array of bioactive constituents that have demonstrated a broad spectrum of pharmacological activities. These include anticancer, antidiabetic, antifungal, antimicrobial, nematocidal, antioxidant, anti-inflammatory, antiallergic, anxiolytic, antihypertensive, anti-obesity, anti-dengue, anti-Alzheimer's, antileishmanial (promastigote), and anti-ulcer properties[26–29]. Based on this, we speculated that diarylnonanoid constituents, particularly the malabaricones, could serve as promising candidates for the development of new therapeutic agents against *N. fowleri*. cinnamon nutmeg, a tree native to Sumatra, Peninsular Malaysia, Singapore, Borneo, the Philippines, and Mindanao, thrives in primary rainforests, mountainous regions, and freshwater swamp forests[1,30]. Commonly known as Mayong Pahomh, Mendarah, Pala Bukit, or Pala Semang[1]. The fruits of the cinnamon nutmeg specifically contain acylphenols such as malabaricones (A-C and E) and dimeric acylphenols known as maingayones (A-B).

In this study, we conducted an *in vitro* analysis of three malabaricone compounds, A-C, against *N. fowleri*. To evaluate potential toxicity to human cells, all compounds were tested on the normal human neuroblastoma cell line (SHSY5Y), while their cytopathogenic effects

were assessed using the HaCat cell line. In parallel, molecular docking studies were performed to identify potential target binding sites, followed by molecular dynamics simulations to predict the interaction of malabaricones with four essential *N. fowleri* proteins: NFCYP51, Cathepsin B, Serine Carboxypeptidase, and Rab family small GTPase. These proteins are critical for the survival of *N. fowleri* and represent promising therapeutic targets for drug development. Additionally, we carried out ADMET (absorption, distribution, metabolism, excretion, and toxicity) predictions to evaluate the safety profile, drug-likeness, and potential side effects of the malabaricone compounds.

2. Materials and Methods

2.1. Chemicals and Reagents

All chemicals used in this study were of analytical grade and obtained from commercial suppliers. Phosphate-buffered saline (PBS) was purchased from Oxoid™ (Basingstoke, UK). Roswell Park Memorial Institute medium (RPMI-1620) and Trypian Blue were sourced from Sigma-Aldrich (St. Louis, MO, USA). Dimethyl sulfoxide (DMSO) was acquired from Thermo Fisher Scientific (Waltham, MA, USA).

2.2. HeLa, HaCaT, and SHSY5Y Cell Culture, Maintenance, and Sub-Culture

The Henrietta Lacks cervical adenocarcinoma cells (HeLa), human keratinocytes (HaCat), and the SHSY5Y cell line were obtained from the American Type Culture Collection (ATCC). Cells were cultured in 75cm^2 tissue culture flasks containing 10 mL of RPMI-1640 medium supplemented with 10% fetal bovine serum (FBS), 1% L-glutamine, non-essential amino acids (NEAA), and 1% penicillin-streptomycin (Pen-Strep). Cultures were maintained in a humidified incubator at 37°C with 5% CO_2 until monolayer formation was observed under an inverted microscope [31]. For subculturing, the spent medium was discarded, and 2 mL of trypsin was added to each flask. Cells were incubated for 10 minutes at 37°C to allow for detachment. Trypsin activity was neutralized by adding fresh supplemented RPMI-1640 medium. The cell suspension was then centrifuged at 1500 rpm for 5 minutes, and the resulting pellet was resuspended in 10 mL of fresh supplemented RPMI-1640 medium.

2.3. N. fowleri Culture and Maintenance

N. fowleri used in this study was clinically isolated from a patient's cerebrospinal fluid and obtained from the American Type Culture Collection (ATCC 30174). The trophozoites were cultured on a monolayer of HeLa cells in 75cm^2 tissue culture flasks,

following previously described protocols[11,31]. Cultures were maintained in 10 mL of RPMI-1640 medium supplemented with penicillin-streptomycin and gentamicin under sterile conditions. RPMI-1640 medium was used consistently to preserve the morphology and viability of *N. fowleri* across all experimental groups. The cultures were incubated at 37°C in a humidified atmosphere containing 5% CO_2.

2.4. Amoebicidal Assay of N. fowleri

N. fowleri trophozoites were harvested from 75cm^2 tissue culture flasks, and anti-amoebic activity was assessed as previously described[31]. Briefly, 2x10^5 trophozoites were seeded into each well of a 24-well clear-bottom plate and treated with malabaricone A-C at concentrations of 25, 50, 75, 100, 150, and 200 µM. Three control groups were included: untreated trophozoites (negative control), trophozoites treated with 100 µM Amphotericin B (positive control), and trophozoites with DMSO (solvent control). All samples were incubated at 37 °C in a 5% CO_2 incubator for 24 hours. Following incubation, cell viability was assessed using the trypan blue exclusion method (0.1%). Viable and non-viable trophozoites were counted using a hemocytometer.

2.5. Cytotoxicity Assay

The cytotoxic effects of malabaricone A-C were evaluated using the SHSY5Y neuroblastoma cell line. SHSY5Y cells were harvested from 75cm² tissue culture flasks and seeded into 96-well clear-bottom plates. After 24 hours of incubation at 37 °C in a 5% CO_2 incubator, a confluent monolayer was formed. The cells were then treated with malabaricone A-C at concentrations of 25, 50, 75, 100, 150, and 200 µM in 200 µL of RPMI-1640 medium. Untreated cells (RPMI only) served as negative control. Following 24 hours of incubation under standard conditions, 1% Triton X (octyl phenol ethoxylate) was added to designated wells as a positive control to induce maximum cell lysis. After an additional 45-minute incubation, the supernatant was collected, and lactate dehydrogenase (LDH) release was quantified using the LDH Cytotoxicity Detection Kit (Roche, Basel, Switzerland). Absorbance was measured at 490 nm using a microplate reader[32]. The percentage of cytotoxicity was calculated using the following formula:

$$\%\boldsymbol{Cytotoxicity} = \frac{\boldsymbol{S_a - NC_a}}{\boldsymbol{PC_a - NC_a}} \times \mathbf{100}\%$$

where S_a is the absorbance of the sample, NC_a is the absorbance of the negative control, and PC_a is the absorbance of the positive control.

2.6. Cytopathogenicity Assay

The cytopathogenic effects of *N. fowleri* were assessed as previously described[31]. Briefly, 2×10^5 *N. fowleri* trophozoites were treated with malabaricone A-C at concentrations of 25, 50, 75, 100, 150, and 200 µM in 24-well clear-bottom plates. The treated trophozoites were incubated for 24 hours at 37°C in a 5% CO_2 incubator. Following incubation, the trophozoites were washed twice with PBS and centrifuged at 3000 rpm for 10 minutes. The supernatant was discarded, and the pre-treated trophozoites were resuspended in 200 µL of RPMI-1640 medium. These pre-treated trophozoites were then added to HaCaT cell monolayers and incubated for an additional 24 hours at 37°C in a 5% CO_2 incubator. Cytotoxicity was assessed by measuring LDH release using the LDH Cytotoxicity Detection Kit (Roche, Basel, Switzerland). The percentage of cell death was calculated using the previously described formula. Two control groups were included: untreated HaCaT cells (negative control) and HaCaT cells treated with 1% Triton X-100 (positive control).

2.7. Statistical Analysis

In the present study, every experiment was performed multiple times. The data is shown as the Mean (of four replicates) ± S.E. (standard error) of two separate tests that were accomplished in duplicate. Microsoft Excel spreadsheet and GraphPad Prism 8.0.1 were used to analyse the gathered data from independent biological evaluations, achieve statistical significance, and Student's *t*-test to compare the impact of tested compounds with solvent control (DMSO). For assessment, * was used to indicate the level of significance for which a *p*-value of less than 0.05 was selected by means of a two-tailed distribution along Student's t-test (two-sample).

2.8. Structure Retrieval and Preparation

Structures of the malabricones A-C, as well as the control amphotericin B, were retrieved from the PubChem database (PubChem IDs 324062, 163001, 100313, and 52809). The existing structure of NFCYP51 was retrieved from the RCSB database (PDB ID 7RKW). The structure was cleaned of any non-protein elements prior to binding site prediction and docking. Sequence structures of cathepsin B, serine carboxypeptidase Nf314, and Rab family small GTPase were downloaded from the UniProt database (UniProt IDs X5D761, P42661, and D2VS55), and the predicted structures were retrieved from AlphaFold.

2.9. Molecular Docking

CB-DOCK2 was used to probe the protein structures of probable binding sites[33,34]. The best three binding sites for each of the proteins were consequently used for docking. Coordinates used were listed in the Table S1. The proteins were cleaned of any bound ligands

and water molecules prior to docking. Each of the four ligands was docked in CB-DOCK2. Furthermore, a second docking software, DINC, was used for the comparison of results[35]. Only results with comparable or greater binding affinity scores than the control was considered for the succeeding steps.

2.10. Molecular Dynamics and Free Binding Energy Calculation

Molecular Dynamics (MD) simulations were primarily done using GROMACS ver.2021.5 simulation software[36,37]. The CHARMM36 force field was used on both protein and ligand[38,39]. Ligand topology was generated using CGENFF following default conditions and parameters[28–30,40,41]. The docked positions were used as the starting position of the simulation and run at 2 2-ps intervals for 50 50-ns simulation time for each of the protein-ligand pairs. Simulation parameters were patterned following Lemkul Lab methods[42].

Molecular Mechanics/Poisson-Boltzmann Surface Area (MM/PBSA) and Molecular Mechanics/Generalized Born Surface Area (MM/GBSA) models were used in calculating free binding energy. Prior to MM/PBSA and MM/GBSA calculations, the simulation box was first centered on the protein, and an index file of 10-frame intervals was generated. The binding energy was calculated using the gmx_MMPBSA tool[43,44]. Using the single-trajectory protocol (STP) from the 500 frames derived from the Gromacs MD trajectory. In brief, the binding energy is calculated using.

$$\Delta G_{bind} = \Delta G_{complex} - (\Delta G_{protein} + \Delta G_{ligand})^{[45]}$$

Where ΔG for each of the terms on the right side of the equation is given by[45]

$$\Delta G = \Delta E_{bonded} + \Delta E_{electrical} + \Delta E_{vdW} + \Delta G_{PB/GB} + \Delta G_{nonpolar}$$

And $\Delta G_{nonpolar}$ is calculated using the solvent accessible surface area model, and $\Delta G_{PB/GB}$ represents either the Poisson-Boltzmann model or the Generalized-born model for MM/PBSA and MM/GBSA, respectively.

Binding energy calculations were performed using gmx_MMPBSA v1.5.0.3 based on MMPBSA version 16.0 and AmberTools 20. Plotting and descriptive statistics were performed using Python 3.10.13 supplemented with modules numpy 1.25.2, pandas 2.0.3, matplotlib 3.7.2, and seaborn 0.13.0.

2.11. ADMET Analysis

ADMET of the malabaricones were also predicted using several models, namely, SwissADME[46], ADMETLab 3.0[47], ProTox 3.0[48,49], and vNN_ADMET[50]. Prediction of

BBB penetration of the malabaricones was carried out using the SwissAMDE's BOILED-Egg model[51,52].

3. Results

3.1. Malabaricone A-C deliver a potent defense against amoebic trophozoites

The amoebicidal assay was carried out to determine the effects of malabaricone A-C on the viability of the *N. fowleri* trophozoites at varying concentrations. The bar graph (Figure 1) shows a steady decrease in viable *N. fowleri* trophozoites as the compound concentration increases. At the highest concentration (200µM), malabaricone B showed the highest amoebicidal activity, in which the number of viable trophozoites was decreased to 8.75×10^4 cells/ mL (73.75%), followed by malabaricone C and malabaricone A having 7.8125×10^4 and 6.5625×10^4 which translates to a 68.75% and 66.25% reduction in viable trophozoites respectively. Moreover, Figure 2 displays the illustrated images of wells from a 24-well plate captured at 200X using an inverted microscope of the effects of malabaricone A-C at 200µM on the viability of *N. fowleri* trophozoites.

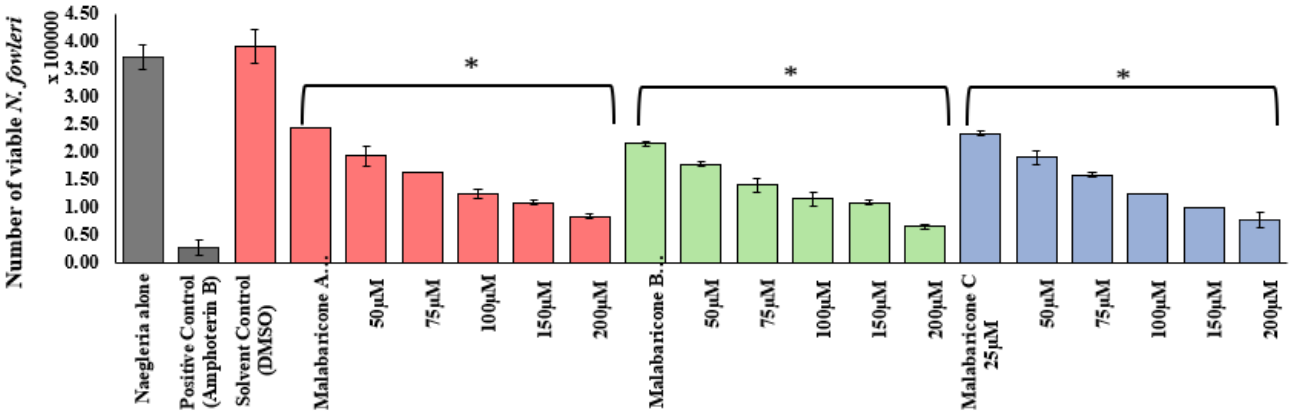

Figure 1. Dose-dependent amoebicidal activity of malabaricone A–C against *N. fowleri* trophozoites. Bar graph showing the viability of *N. fowleri* trophozoites after 24-hour treatment with increasing concentrations (25, 50, 75, 100, 150, and 200 µM) of malabaricone A-C. Viability was assessed using Trypan blue exclusion and quantified via hemocytometer. Amphotericin B (100 µM) served as the positive control, while untreated and DMSO-treated trophozoites were used as negative and solvent controls, respectively. Results are expressed as mean ± standard error (n = 4). Asterisks (*) indicate statistically significant differences compared to the solvent control ($p < 0.05$, using two-sample T-test, two-tailed distribution). Malabaricone B exhibited the highest amoebicidal activity, followed by C and A.

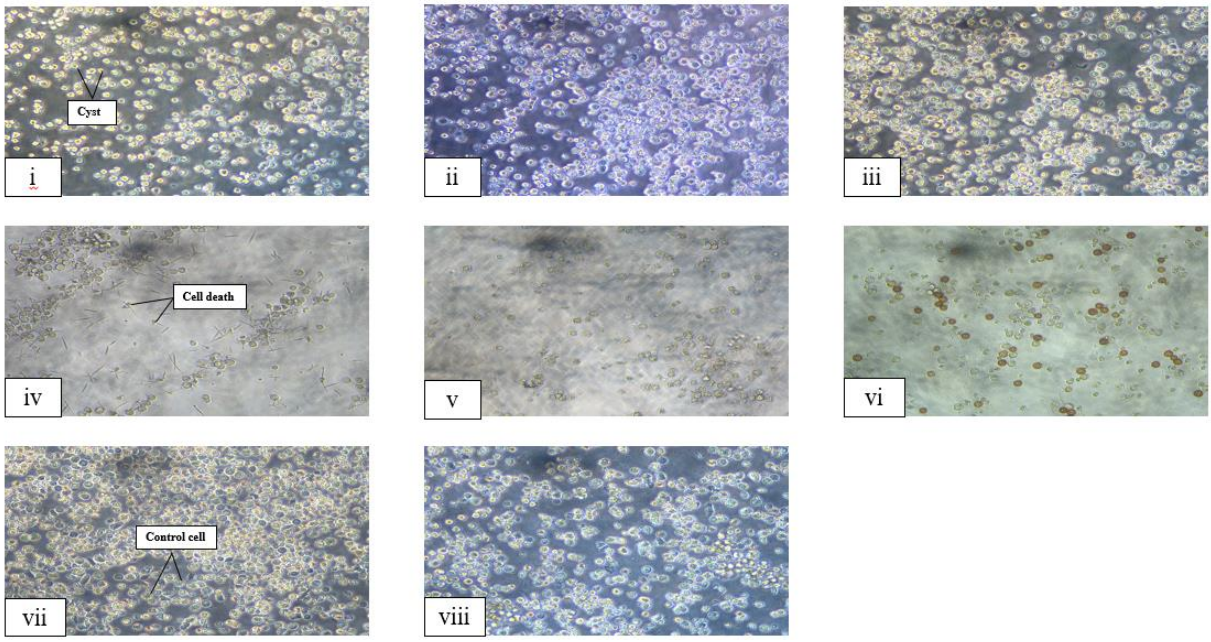

Figure 2. Microscopic visualization of *N. fowleri* trophozoites treated with malabaricone A–C**.** Representative images captured at 200× magnification using an inverted microscope show morphological changes in *N. fowleri* trophozoites after 24-hour exposure to malabaricone A–C. Panels (i–iii) show trophozoites treated with 25 µM of malabaricone A-C, respectively. Malabaricone B-treated cells (panel ii) exhibit pronounced rounding, cytoplasmic condensation, and membrane deformation, indicating advanced stages of stress or cell death. Malabaricone C-treated cells (panel iii) show marked loss of structural integrity, severe membrane blebbing, extensive cell shrinkage, and cellular debris formation, consistent with late-stage apoptosis or necrosis. These effects highlight malabaricone C as the most potent compound in inducing amoebicidal activity. Panels (iv–vi) show trophozoites treated with 200 µM of malabaricone A-C, respectively. Panel (vii) shows untreated trophozoites (negative control), and panel (viii) shows DMSO-treated trophozoites (solvent control). Treated cells across all conditions exhibit membrane disruption and reduced density, consistent with cell death.

3.2. Natural Compounds Exhibit Cytopathogenic Effect Inhibition with Minimal Toxicity in SH-SY5Y Cells

The cytotoxicity assay was carried out to determine the toxicity of the natural compounds (To evaluate the safety profile of natural compounds—malabaricone A, B, and C—a cytotoxicity assay was conducted using the SH-SY5Y cell line (Figure 3A). The LDH assay revealed that all three compounds exhibited low toxicity (<20%) at concentrations of 25 µM, 50 µM, and 75 µM. However, at a higher concentration of 200 µM, malabaricone A showed the highest cytotoxicity (50.45%), followed by malabaricone B (44.61%) and malabaricone C (30.26%).

In parallel, the cytopathogenicity assay was performed to assess the compounds' ability to mitigate the amoebic effects of Naegleria fowleri on HaCaT cells (Figure 3B).

Trophozoites pretreated with increasing concentrations of malabaricone A–C demonstrated a dose-dependent reduction in cytopathogenicity. Untreated N. fowleri trophozoites induced 33.43% sensitivity in HaCaT cells, whereas pretreatment with malabaricone C resulted in the lowest cytopathogenicity (7.93%) at 200 µM, followed by malabaricone B (9.42%) and malabaricone A (11.28%). These findings suggest that malabaricone derivatives not only exhibit minimal toxicity at lower concentrations but also effectively reduce *N. fowleri*-mediated cytopathogenic effects, highlighting their potential as therapeutic candidates for both instances as displayed via the cytotoxicity assay in Figures 3A & B.

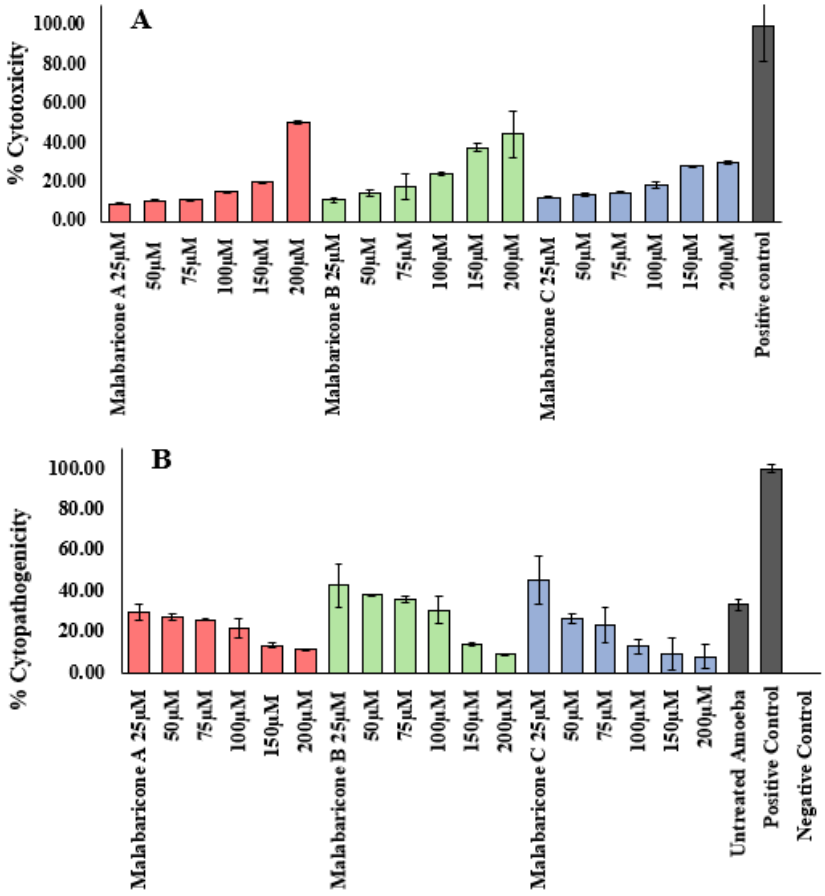

Figure 3. Cytotoxicity and anti-cytopathogenic effects of malabaricone A–C. Bar graphs illustrating (A) the cytotoxicity of malabaricone A–C on SH-SY5Y human neuroblastoma cells and (B) the inhibition of *N. fowleri*-induced cytopathogenicity in HaCaT keratinocyte monolayers. In panel (A), SH-SY5Y cells were treated with malabaricone A–C at concentrations ranging from 25 to 200 µM for 24 hours. Cytotoxicity was assessed using the LDH release assay, with Triton X-treated cells as the positive control and untreated cells as the negative control. All compounds exhibited minimal cytotoxicity (<20%) at lower concentrations (25–75 µM). At 200 µM, malabaricone A showed the highest cytotoxicity (50.45%), followed by B (44.61%) and C (30.26%). In panel (B), *N. fowleri* trophozoites were pre-treated with the same compound concentrations before co-incubation with HaCaT cells for 24 hours. Cytopathogenicity was measured via LDH release. Untreated HaCaT cells served as the negative control, while Triton X-treated cells were the positive control. All compounds significantly reduced cytopathogenicity in a dose-dependent manner. At 200 µM, malabaricone C demonstrated the greatest protective effect (7.93%), followed by B (9.42%) and A (11.28%). Data are presented as mean ± standard error ($n = 4$), with * indicating $p < 0.05$.

3.3. In silico Assessments of Malabaricones

3.3.1. Molecular binding energies estimation

To gain insights into the potential mechanisms of action of malabaricones against *N. fowleri*, we conducted *in silico* analyses of their interactions with four target proteins critical to amoebic viability: sterol 14α-demethylase (NFCYP51), serine carboxypeptidase (Nf314), Rab family small GTPase, and cathepsin B. These targets were selected based on their known virulence roles and sequence conservation in pathogenic amoebae. Initial molecular docking, summarized in Table S2, identified plausible binding poses for each malabaricone across these targets. Cathepsin B exhibited consistently lower binding scores relative to the control, suggesting weaker interactions, while the remaining three targets showed favourable docking interactions with all malabaricones.

Importantly, docking was not used to infer relative binding affinities or rank compound potency. Instead, it served as a preparatory step to generate initial ligand–protein conformations for 50-ns molecular dynamics (MD) simulations, from which binding stability and energetics were rigorously assessed via MM/PBSA and MM/GBSA methods. The resulting binding free energies are summarized in Table 1, with expanded data in Table S3.

Table 1. Gromacs for a 50-ns MD simulation to determine binding stability and for the calculation of free binding energies using MM/PBSA and MM/GBSA methods.

	ΔGbind in kJ/mol			
Complex	**$\bar{x}$ ±CI^a**	**SE**	**Mode**	**Minima**
CYP-MA	1.846 ± 0.383	0.195	1.14	-10.16
CYP-MB	11.569 ± 0.411	0.209	12.39	-3.15
CYP-MC	5.279 ± 0.480	0.245	5.86	-11.01
R-MA	4.288 ± 0.453	0.231	3.67	-7.11
R-MB	**-3.263 ± 0.585**	**0.298**	**-9.03**	**-18.97**
R-MC	5.034 ± 0.770	0.392	2.89	-15.79
S-MA	**-4.873 ± 0.967**	**0.492**	**-13.9**	**-25.27**
S-MB	**-2.229 ± 0.596**	**0.303**	**-3.25**	**-18.75**
S-MC	**-1.217 ± 0.531**	**0.270**	**-2.24**	**-20.44**

Standard error, SE; NFCYP51, CYP; serine carboxypeptidase Nf314, S; Rab family small GTPase, R; malabaricone A, MA; malabaricone B, MB; malabaricone C, MC.[a]At α=0.05

The binding energies computed using MM/GBSA were systematically more negative (i.e., more favourable) than those from MM/PBSA. This reflects the inherent methodological differences between the two algorithms: The Generalized Born (GB) model used in MM/GBSA applies analytical approximations to estimate solvent effects, making it computationally efficient but prone to optimistic bias. Conversely, MM/PBSA employs a Poisson–Boltzmann (PB) numerical solution that is more computationally intensive but offers a more conservative and precise estimation of polar solvation—frequently resulting in less favourable (or more positive) ΔG values.

Despite these differences, both methods consistently identified serine carboxypeptidase as the most energetically favourable binding partner across all malabaricones. The MM/GBSA approach showed universally negative ΔG_{bind} values for all nine ligand–protein complexes. In contrast, MM/PBSA identified spontaneous (i.e., negative ΔG) binding in only four complexes: malabaricone B with Rab GTPase (R-MB) and malabaricone A-C with serine carboxypeptidase (S-MA, S-MB, S-MC). Several of the MM/PBSA energy distributions, plotted in Figure 4 and Figure S1, exhibited multimodal behavior. Most pronounced of these is the S-MA complex, showing a pronounced dual-peak distribution, with a higher-probability mode at negative ΔG and a secondary mode at positive ΔG. This suggests the existence of two dominant protein–ligand binding states—one representing favourable, stable binding and the other less favourable or unstable. A similar pattern was observed for the R-MB complex, although its lesser peak hovered around neutral ΔG, indicating a high likelihood of at least moderate binding.

These energetic trends align closely with the *in vitro* phenotypes. Malabaricone B, which produced the highest amoebicidal activity (73.75% trophozoite inhibition at 200 µM) in this study *in vitro*, also demonstrated stable and energetically favourable binding to both serine carboxypeptidase and Rab GTPase in MM/PBSA analyses. Malabaricone A, which showed the weakest *in vitro* activity, correlated with a bimodal ΔG distribution for S-MA where an unfavourable (positive ΔG) state was clearly populated—possibly reflecting weaker or transient target engagement.

Detailed structural analysis (Figure S2) further supports these findings. In the unfavourable binding state of malabaricone A with serine carboxypeptidase (positive ΔG), only non-specific van der Waals contacts were observed. In contrast, the favourable binding state included three hydrogen bonds involving His308, Glu326, and Ser312, in addition to van der Waals forces. Notably, His308 served as a shared contact point across all malabaricones. The stronger performance of malabaricone B and C may be attributed to additional hydroxyl groups on their tail rings, which facilitated increased hydrogen bonding,

although the interaction patterns varied in frequency across the simulation trajectory (Figures S3, Figure S4).

For the R-MB complex, the para-position hydroxyl group on malabaricone B consistently formed hydrogen bonds with Ser149, Ala150, and Lys151, reinforcing the stability of this complex (Figure S5). These stable and targeted interactions likely contribute to favourable energetics and support malabaricone B's superior amoebicidal action.

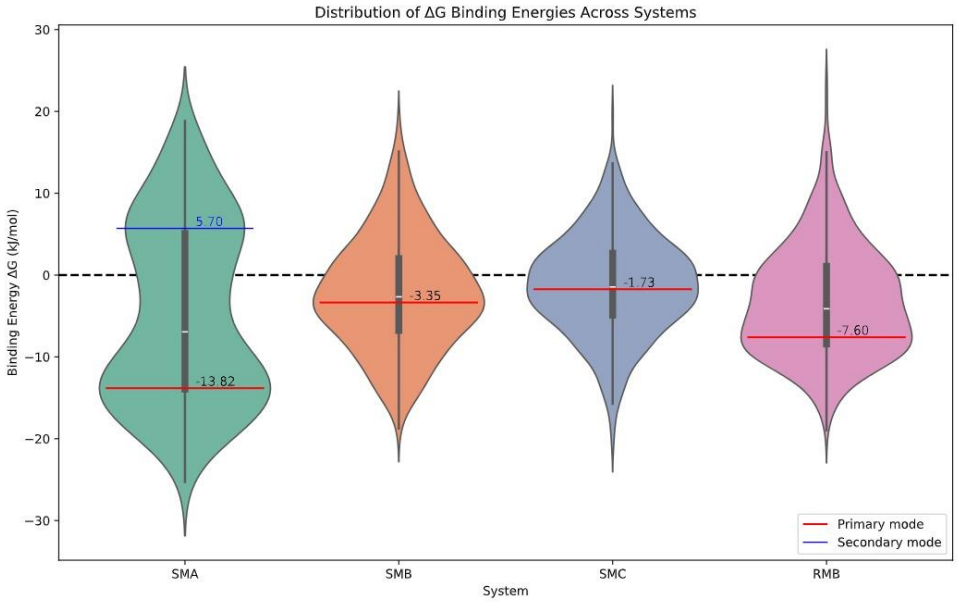

Figure 4. ΔG Binding Energy Landscape of malabaricone A-C with serine carboxypeptidase (SMA, SMB and SMC, respectively), and malabaricone B with Rab family GTPase (RMB). Distribution of MM/PBSA ΔG binding energies for malabaricone–protein complexes, as generated from 50-ns molecular dynamics (MD) simulations. The violins display the full spectrum of calculated binding free energies, where the shape denotes the density at each ΔG value. The central box plot (dark gray) within each violin shows the median and interquartile range. Thick horizontal red and blue lines denote kernel density-derived primary and secondary modal binding energies, respectively (labeled with corresponding values). A horizontal dashed line indicates ΔG=0kJ/mol. All data reflect frame-wise energies computed via GROMACS v2021.5 using the CHARMM36 force field**.**

3.3.2. ADMET properties of natural-based compounds

Since *N. fowleri* directly invades brain tissue via the olfactory nerves, an essential pharmacokinetic consideration is whether candidate compounds can be absorbed from the gastrointestinal tract and reach the central nervous system. Structure-based predictions (Table 2, Figure 5**)** indicate that all three malabaricone A-C have high predicted human intestinal absorption (HIA) and gastrointestinal absorption (GIA). Both Caco-2 and MDCK models predict favourable permeability, suggesting efficient passage across epithelial layers. While Caco-2 reflects passive diffusion through intestinal tissue, MDCK evaluates both passive and active transport, including potential efflux mechanisms. The slightly lower MDCK scores

may reflect the predicted P-glycoprotein-negative (PGP-) status of all three compounds, indicating minimal risk for efflux by intestinal transporters. Together, these data suggest that malabaricones are likely absorbed via passive membrane diffusion, supported by suitable lipophilicity and favourable permeability profiles. Nonetheless, their low predicted water solubility may pose formulation challenges for oral delivery.

Among the three, malabaricone A is uniquely predicted to penetrate the BBB, based on its polarity and lipophilic balance, making it a promising candidate for treating N. fowleri, which resides in the CNS (Figure 5). In contrast, malabaricone B and C, although more pharmacologically potent *in vitro*, may lack CNS penetration unless formulation strategies or delivery systems are applied to enhance brain uptake. All malabaricones demonstrated high plasma protein binding (PPB) probabilities, which may reduce free circulating drug concentrations and potentially affect therapeutic availability or clearance rates.

Metabolic liability was assessed through predicted interactions with cytochrome P450 (CYP) enzymes. All three malabaricones exhibit multiple CYP "hits", implying a high probability of metabolism via hepatic enzymes, particularly CYP inhibition. While CYP binding suggests susceptibility to metabolic breakdown, CYP inhibition raises concerns for potential drug–drug interactions or off-target toxicity. As ideal candidates should neither strongly bind to nor inhibit CYP isoforms, further structure optimization may be needed to mitigate metabolic risks.

High PPB levels also suggest prolonged circulation of half-lives, but may compromise renal or hepatic clearance, warranting in vivo studies on pharmacokinetic profiles. Although detailed renal clearance models were not part of the current work, the predicted non-substrate status for PGP favors cellular uptake and reduces the likelihood of rapid efflux, supporting potential systemic accumulation.

Tables 3 and S4 compare toxicity predictions from three *in silico* platforms—ADMETLab 3.0, ProTox, and vNN-ADMET. All malabaricones were consistently classified as non-mutagenic and non-carcinogenic by all models. ADMETLab and vNN-ADMET also predicted that none of the malabaricones are hERG blockers, suggesting low risk for cardiac arrhythmias linked to QT prolongation. However, ProTox flagged all compounds, including amphotericin B, as potentially cardiotoxic—suggesting possible non-hERG related cardiotoxicity pathways requiring further *in vitro* or *in vivo* clarification.

Regarding nephrotoxicity, ADMETLab predicted a low probability of kidney toxicity across all malabaricones, whereas ProTox labeled them as "active," with moderate risk

probabilities of 61–63%. This discrepancy likely stems from differing modeling methods and training data: ADMETLab uses graph-based neural networks (DMPNN) and chemically comprehensive descriptors[53], while ProTox relies on traditional machine learning, structural analogues, and toxicophore-based alerts[54,55]. Supporting the ADMETLab prediction, Li report that malabaricone B and C showed no acute renal toxicity *in vitro*. However, Li found that long-term administration of nutmeg powder, which contains malabaricones, induced renal and hepatic changes in mice, suggesting potential cumulative effects with chronic exposure. For drug-induced liver injury (DILI), both ADMETLab and ProTox classified the compounds as safe [56].

Notably, ADMETLab predicted a high probability of respiratory irritation for all three malabaricones, whereas ProTox only identified malabaricone B as a potential respiratory irritant. These conflicting results may be model-specific and less relevant for a disease primarily affecting the central nervous system. Nonetheless, they highlight the need for targeted inhalation or mucosal safety studies in future investigations, especially if intranasal delivery routes are considered.

Finally, none of the malabaricones violated Lipinski's Rule of Five, reinforcing their drug-like properties. By contrast, amphotericin B, a current anti-*N. fowleri* drug violates at least one rule and cannot be evaluated by SwissADME due to size limitations in SMILES-based computation (>200 characters).

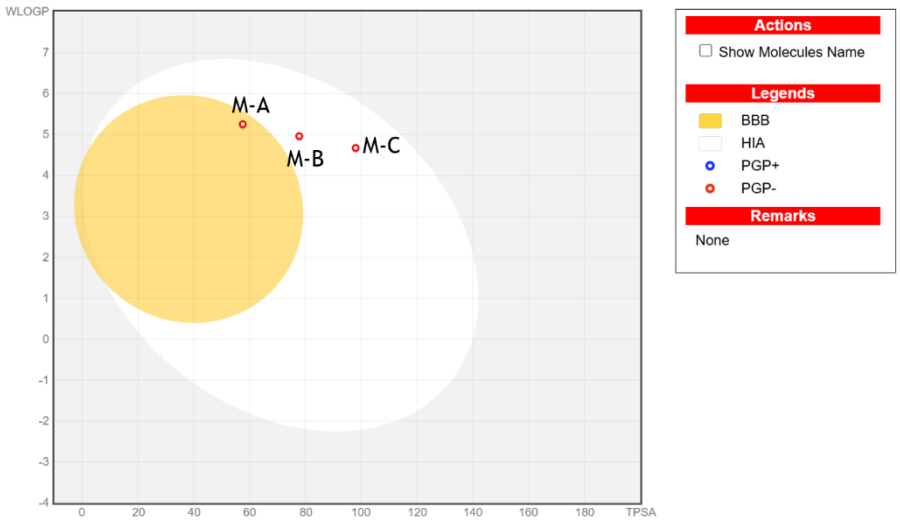

Figure 5. BOILED-Egg model of absorption and penetration by SwissADME. The egg white indicates gastrointestinal tract penetration, and the egg yolk indicates BBB penetration. Red circles indicate PGP-negative; the molecules were predicted not to be substrates of the P-glycoprotein efflux transporters. Malabaricone A is indicated as M-A, B as M-B, and C as M-C.

Thus, malabaricones offer several pharmacokinetic and safety advantages over current therapies: they have favourable absorption, better potential for brain penetration, and

a safer *in silico* toxicity profile, especially compared to amphotericin B and miltefosine. Experimental studies are warranted to confirm these translational predictions and resolve inter-model discrepancies, especially around nephrotoxicity and respiratory irritation.

Table 2. Summary of ADME results for malabaricone A, B, C, and amphotericin B using SwissADME and ADMETLab3.0 prediction models.

		Mal A		**Mal B**		**Mal C**		**Amphotericin B**		**Miltefosine**		**Nitroxoline**	
	desirable values	**Swiss ADME**	**ADMET Lab3.0**	**Swiss ADME**	**ADMET Lab3.0**	**Swiss ADME**	**ADMET Lab3.0**	***Swiss ADME**	**ADMET Lab3.0**	**Swiss ADME**	**ADMET Lab3.0**	**Swiss ADME**	**ADMET Lab3.0**
Lipophilicity (logP/logD)	<5	4.81	1.57	4.36	2.77	3.93	1.42	nd	0.51	3.35	0.77	1.01	0.95
water solubility (logS)	>-4	poor	-4.16	poor	-3.58	poor	-3.52	nd	-2.68	poor	-0.85	soluble	-3.29
GIA / HIA		high	high	high	high	high	high	nd	high	low	low	high	high
Caco-2	>-5.15	nd	-4.99	nd	-4.99	nd	-4.94	nd	-5.78	nd	-5.39	nd	-4.87
MDCK	>-4.70	nd	-4.66	nd	-4.68	nd	-4.67	nd	-5.33	nd	-4.74	nd	-4.36
PGP substrate		no	no	no	no	no	no	nd	no	yes	no	no	no
BBB penetration	>0.50	yes	0.61	no	0.06	no	0.07	nd	2.12e-12	no	<0.01	no	<0.01
bioavailability	>30%	55%	50%	55%	50%	55%	50%	nd	50%	55%	50%	55%	<20%
PPB	<90%	nd	99%	nd	98%	nd	98%	nd	63%	nd	98%	nd	94%
CYP binding	0	nd	3/6	nd	3/6	nd	4/6	nd	0/6	nd	3/6	nd	2/6
CYP inhibitor		5/5	5/7	5/5	6/7	5/5	6/7	nd	0/7	2/5	4/7	1/5	1/7
Lipinski	accept (0)	0	accept	0	accept	0	accept	nd	reject	0	accept	0	accept

*Amphotericin could not be run in SwissADME due to its SMILES structure hitting the limit of 20 characters maximum GIA – gastrointestinal absorption; HIA – human intestinal absorption; Caco-2 – human colorecta adenocarcinoma test; MDCK – Madin-Darby canine kidney assay; PGP – P-glycoprotein; PPB – plasma protein binding; CYP – Cytochrome p450; nd – no data, the model did not include the parameter or the molecule could not be run in the model. logP, logD, and logS are unitless logarithmic values; Caco-2 and MDCK are in log(cm/s); bioavailability and plasma protein binding (PPB) are reported as percentages. For water solubility, logS values less than -4 are considered poorly soluble, indicating solubility <100 µM

Table 3. Summary of toxicity predictions for malabaricone A, B, C, and amphotericin B using ADMETLab3.0 and ProTox models.

		Mal A		**Mal B**		**Mal C**		**Amphotericin B**		**Miltefosine**		**Nitroxoline**	
		ADMET Lab	ProTox	ADMET Lab	ProTox	ADMETLab	ProTox	ADMET Lab	ProTox	ADMET Lab	ProTox	ADMET Lab	ProTox
hERG blocker	<50 %	28%	nd	23%	nd	15%	nd	0%	nd	7%	nd	7%	nd
Cardiotoxicity	<50 %	nd	active	nd	active	nd	active	nd	active	nd	inactive	nd	inactive
Ames Toxicity	<50 %	23%	nd	23%	nd	29%	nd	56%	nd	2%	nd	92%	nd
Mutagenicity	<50 %	nd	inactive	nd	inactive	nd	inactive	nd	inactive	nd	inactive	nd	active
Carcinogenicity	<50 %	10%	inactive	15%	inactive	13%	inactive	2%	inactive	96%	inactive	63%	active
ROA / cytotoxicity	<50 %	22%	inactive	24%	inactive	27%	inactive	<1%	inactive	76%	inactive	53%	inactive
Nephrotoxicity	<50 %	34%	Active, 61%	23%	Active, 63%	10%	Active, 61%	100%	Active, 77%	100%	inactive	35%	inactive
Hepatotoxicity / DILI	<50 %	7%	inactive	4%	inactive	10%	inactive	53%	inactive	5%	inactive	92%	active
Neurotoxicity	<50 %	16%	inactive	14%	inactive	2%	inactive	0%	inactive	22%	inactive	13%	inactive
Respiratory irritation	<50 %	94%	inactive	94%	active	92%	inactive	0%	active	100%	active	93%	inactive

hERG – a human K+ ion channel in the heart, used for cardiotoxicity marker; DILI – drug-induced liver injury; ROA – rat acute oral toxicity; active – drug has predicted toxicity; inactive – drug is safe or not flagged for toxicity; nd – no data. Qualitative descriptors (e.g., "active", "inactive") are end-point predictions based on in silico models.

4. Discussion

N. fowleri is found globally except in Antarctica, with a higher prevalence in regions characterized by warm climates and abundant warm freshwater bodies. Given Malaysia's tropical climate and the widespread presence of water bodies often used for recreational activities such as swimming, the risk of exposure to the amoeba is heightened[57,58]. Understanding *N. fowleri* infections and associated precautions is essential, especially since the risk may emerge at any time despite no recorded cases to date[57]. Supporting this concern,

a study revealed that over 70% of water samples collected from 11 Malaysian states contained *Naegleria spp.*[59]. This highlights the importance of precautionary measures and available treatment options, prompting ongoing research into natural compounds like malabaricone, which has shown promise in combating various microbial infections.

Malabaricone A–D are classified as diarylnonanoids or phenylacylphenols, a group of secondary metabolites isolated from plants in the *Myristicaceae* family. These compounds are characterized by nine carbon atoms linking two aromatic rings and are known for their distinctive bioactive properties[60,61]. Due to their unique structural features and diverse pharmacological activities, malabaricones have attracted considerable scientific interest [61]. In the present study, the effect of malabaricone on *N. fowleri* was assessed, with promising results. Although the precise mechanism by which malabaricone acts on amoeba remains unknown, this study provides a valuable foundation for future investigations. The anti-amoebic analysis of malabaricones demonstrated that all three compounds effectively inhibited the viability of trophozoites, suggesting strong potential for development as therapeutic agents against PAM infection. Among them, malabaricone B exhibited the highest inhibitory activity, followed by malabaricone C and A. Structural analysis revealed that malabaricone A–C differs in the number and position of hydroxyl (-OH) groups on the second benzene ring. Specifically, malabaricone A lacks an -OH group, while malabaricones B and C contain one and two -OH groups, respectively[62–64]. The presence, number, and position of hydroxyl (-OH) groups appear to play a crucial role in the anti-amoebic activity of malabaricones. Malabaricone C, which contains -OH groups at positions C13 and C14, exhibited the strongest activity, followed by malabaricone B with a single -OH group at C14.

In contrast, malabaricone A, which lacks any -OH groups, showed the weakest effect. Mechanistic studies using molecular dynamics simulations and binding energy calculations indicate that the -OH groups in the second benzene ring may have played a role in the binding of malabaricones to the target proteins (Figure S3–S5). These findings are consistent with the study by Ahmed[65], which also reported that malabaricone induces necrotic cell death in free-living amoebae. In contrast, malabaricone A was comparatively less effective, exhibiting only moderate anti-amoebic activity. This observed potency coincides with previous findings in *A. castellanii*, where malabaricone C demonstrated nearly twice the efficacy of malabaricone B in inhibiting amoebal growth[25].

Malabaricone has also demonstrated the ability to induce apoptotic cell death in triple-negative breast cancer (TNBC) cell lines by triggering nuclear fragmentation[66]. These findings, along with previous studies, suggest that malabaricone can induce either apoptotic

or necrotic cell death in both amoebae and human cancer cell lines. In the case of HaCaT, SHSY5Y cells, or *N. fowleri*, the mode of cell death, whether apoptotic or necrotic, remains uncertain[65,66]. As this study did not specifically investigate the mechanism of cell death, it is postulated that malabaricone may act through nuclear fragmentation via either intrinsic or extrinsic apoptotic pathways. Additionally, another study reported that malabaricone A exhibited pro-oxidant activity, leading to cytotoxicity in leukemic cells by inducing oxidative stress and activating caspase-dependent apoptosis[67]. Given the multiple potential mechanisms through which malabaricone may induce cell death, further research is necessary to elucidate its exact pathways and modes of action.

Cytotoxicity assessment is essential[68,69], and in the present study, SHSY5Y, was used to evaluate the toxicity of the tested compounds (Figure 3A), exhibited minimal cytotoxicity. In a previous study conducted by Usman *et. al*[65] toxicology validation upon the HaCaT cells with malabaricone had similar findings. Since *N. fowleri* typically enters the body through the nasal passage, keratinocytes serve as a primary barrier. HaCaT cells, which are immortalized human keratinocytes with near-normal phenotypes, are well-suited as a model for studying barrier function against pathogens and drugs[70]. Given that infection ultimately affects the CNS, malabaricone toxicity was also assessed using the SHSY5Y neuroblastoma cell line. Both cell lines, SHSY5Y and HaCaT[65] exhibited low toxicity at lower concentrations of malabaricone, but increased cell death was observed at higher concentrations. These findings are consistent with previous studies showing that malabaricones, particularly malabaricone C, exhibit selective cytotoxicity and anti-inflammatory effects without compromising cell viability at therapeutic doses. For example, malabaricone C was shown to inhibit T-cell proliferation and cytokine secretion while maintaining low toxicity in lymphocytes, suggesting its potential for immunomodulatory applications[71]. In contrast, other natural compounds such as plumbagin and menadione, though effective as pro-oxidants, demonstrated higher cytotoxicity at sub-micromolar concentrations, limiting their therapeutic window[72].

To evaluate the protective potential of the test compounds against *N. fowleri*-induced cytopathogenicity, HaCaT keratinocyte monolayers were co-incubated with trophozoites pre-treated with each compound. Cytotoxicity was quantitatively assessed through lactate dehydrogenase (LDH) release, a well-established marker of membrane damage. As expected, untreated HaCaT cells showed minimal LDH release, serving as a negative control, while treatment with Triton X elicited maximal cytolysis, validating the assay as a positive control. All three malabaricones A-C demonstrated a significant, dose-dependent reduction in cytopathogenicity, indicating that pre-treatment of *N. fowleri* trophozoites impaired their

ability to cause host cell damage (Figure 3B). These findings support the hypothesis that malabaricones can attenuate *N. fowleri*'s cytopathic effects on human epithelial cells, potentially by interfering with parasite viability, adhesion, or secreted virulence factors

Compared to these agents, malabaricones offer a more favourable safety profile, from their ADMET and toxicology prediction results and in epithelial and neuronal models like HaCaT and SHSY5Y. This supports their potential as safer alternatives for targeting *N. fowleri* infections, particularly in tissues vulnerable to amoebic invasion.

While in silico ADMET models predicted that malabaricone A is most likely to cross the blood-brain barrier, malabaricone B demonstrated superior in vitro anti-amoebic activity. This apparent difference reflects the distinct evaluation criteria of computational pharmacokinetic profiling and cell-based efficacy testing. To fully realize the therapeutic potential of malabaricones B and C as CNS-targeted agents, future development may leverage advanced drug delivery approaches to enhance brain uptake and clinical effectiveness. A recent study on polymeric nanocarriers demonstrated efficient microglial payload delivery in animal models which future studies could utilize for systemic administration *in vivo*[73]. Lipid-based nanocarriers like liposomes and micelles could also be used to enable malabaricones B and C to reach the target site[74,75]. Further enhancement, either by conjugation or functionalization of carrier can further improve drug delivery, like borneol and menthol, which were shown to enhance targeting and brain penetration[76,77]. Intranasal administration could also be done to enhance delivery and circumvent poor systemic bioavailability predicted for the malabaricones. Finally, future studies could design a pro-drug form that would ensure reaching the target site and efficient transformation into the drug's potent amoebicidal forms.

Further research could explore strategies to reduce malabaricone's toxicity in human cells, potentially through synergistic effects at lower doses. Notably, malabaricone C, identified as the most effective compound in protecting HaCaT cells against *N. fowleri*, also showed the lowest toxicity at 200 µM compared to malabaricone A and B, which is a promising outcome. Additionally, previous studies (data not shown) indicated that malabaricone exhibited minimal toxicity in HeLa cells[70]. Since nucleases cleave nucleic acids by hydrolyzing phosphodiester bonds, this activity may have contributed to nuclear damage in *N. fowleri* observed in the present study[78]. These findings further support the hypothesis that malabaricone's amoebicidal activity, whether apoptotic or necrotic, may be linked to disruption of genetic material.

CYP51 (sterol 14α-demethylase) is a cytochrome P450 enzyme that plays a critical role in sterol biosynthesis[79,80]. Pharmacological studies have shown that thymol interacts with ergosterol, a key structural component of the *N. fowleri* membrane[81]. Sterol biosynthesis is essential to produce cholesterol in mammals and ergosterol in fungi, both of which are vital for maintaining membrane integrity. In *N. fowleri*, ergosterols are crucial lipids found in the plasma membrane, supporting amoeboid survival[56, 57]. It is postulated that malabaricone may exhibit a similar mechanism of action. The principle of targeting ergosterol biosynthesis offers a promising strategy to inhibit amoebae without adversely affecting the host[82]. Accordingly, the present study employed *in silico* validation focusing on CYP51 as the molecular target, further suggesting a potential mechanism of action for malabaricone against *N. fowleri*.

A study by Herbst reported that extracts from both intact and free-cell amoebae exhibit cytolytic and tissue-destructive activity[83]. These effects are attributed to various factors, including phospholipases, undefined hemolytic agents, and a secreted cysteine proteinase identified as the most potent contributor to tissue damage through pore formation in target cell membranes[83]. Their research also revealed that glycoproteins possess strong pore-forming capabilities, with these polypeptides capable of killing both prokaryotic and eukaryotic cells[83]. A similar mechanism may have occurred in the present study, although this cannot be confirmed without further investigation.

It would be valuable to explore whether malabaricones can target and disrupt these polypeptides in *N. fowleri.* Supporting this possibility, malabaricone A has been shown to exert cytotoxic effects on leukemic and multiple myeloma cell lines, regardless of their P-glycoprotein (P-gp) activity levels[84]. During infection, *N. fowleri* is known to activate a cascade of inflammatory pathways, which can lead to the degradation of extracellular matrix (ECM) components and the generation of oxidative stress through reactive oxygen species (ROS)[60,61].

The antioxidant and anti-inflammatory properties of malabaricone compounds warrant further investigation in the context of *N. fowleri* infection. Previous studies have reported that malabaricones exhibit potent ROS scavenging activity and suppress pro-inflammatory cytokines[85]. Understanding these effects could help elucidate the precise mechanism of malabaricone action. By mitigating ROS and preserving the extracellular matrix (ECM), malabaricone may offer protective benefits during *N. fowleri* infection. However, additional *in vitro* and *in vivo* studies are necessary to confirm these effects. Although not yet proven, the protective effect observed in HaCaT cells in the present study

may be attributed to the antioxidant and anti-inflammatory properties of malabaricone, as suggested by earlier findings. Recent findings have shown that malabaricone C (Mal C) significantly inhibits mitogen-induced T-cell proliferation and cytokine secretion, including IL-2 and IFN-γ, by modulating cellular redox states and suppressing NF-κB activation[71,72,86,87]. Mal C also reduced intracellular thiol levels in lymphocytes, and its effects were reversed by N-acetyl cysteine (NAC), confirming its redox-dependent mechanism[71,87,88].

5. Conclusions

Among the tested compounds, malabaricone B emerged as the most promising candidate, showing potent anti-amoebic activity by significantly reducing *N. fowleri* trophozoite viability and cytopathogenicity. Malabaricone B also demonstrated notable efficacy, while malabaricone A showed potential for central nervous system delivery due to its predicted ability to cross the blood-brain barrier. These *in vitro* findings were supported by *in silico* analyses, which revealed favourable interactions between the malabaricones and key *N. fowleri* proteins, including serine carboxypeptidase and Rab family small GTPase, aligning well with observed anti-amoebic effects. All compounds displayed low cytotoxicity toward human cells at effective concentrations, and ADMET profiling indicated a low risk of nephrotoxicity and genotoxicity, though improvements in bioavailability may be needed.

This study expands the repertoire of natural compounds with efficacy against a highly lethal and neglected pathogen. By identifying malabaricones, particularly malabaricone B, as promising lead scaffolds, it lays a strong foundation for developing safer, targeted treatments for PAM. In doing so, it contributes directly to the advancement of Sustainable Development Goal 3 (Good Health and Well-being) by supporting the discovery of effective therapies for neglected infectious diseases and promoting global health equity. Furthermore, Sustainable Development Goal 12 (Responsible Consumption and Production) is advanced by leveraging digital innovation to reduce experimental waste and optimize resource use in the development of novel therapeutics. Continued preclinical and clinical investigations will be essential to fully realize the therapeutic potential of these acylphenol compounds in addressing the urgent medical challenge posed by the “brain-eating” amoeba.

Author Contributions: KR, LT: developed and supervised the study; LT, MG, SWC, RCM: Data curation, Formal analysis, Investigation, Writing — original draft; DA, MAO: analysis of the natural compounds; YS, AA, HT, CIJ: wrote- original draft, project administration, resources, conceptualisation, funding acquisition, and writing — review & editing; KR, NKK, UA: experiments against *N. fowleri*.

Funding: This research work was supported by Sunway University Malaysia (Cintana Grant, GRTEX-INT-DADTP-CINTANA-2024-001).

Acknowledgements: The successful completion of this research was made possible through the substantial support and collaboration of multiple institutes. We showed our deepest gratitude to Sunway University, Malaysia; Mapua University, Philippines, and University Malaya, Malaysia. We sincerely appreciate the efforts of all co-authors, faculty members, and researchers. Special thanks to Yee Mon Htet for her valuable assistance in the design and alignment of all figures and tables.

Conflicts of Interest: The authors disclose that they do not have any conflicts of interest.

References

1. Ong KS, Letchumanan V, Law JWF, *et al.* Microbes from peat swamp forest — the hidden reservoir for secondary metabolites? Prog Microbes Mol Biol 2020;3(1).
2. Siddiqui R, Khan NA. Biology and pathogenesis of *Acanthamoeba*. Parasites Vectors 2012;5.
3. Naveed M, Ali U, Aziz T, *et al.* Development and immunological evaluation of an mRNA-based vaccine targeting *Naegleria fowleri* for the treatment of primary amoebic meningoencephalitis. Sci Rep 2023;13.
4. Chaúque BJM, dos Santos DL, Anvari D, *et al.* Prevalence of free-living amoebae in swimming pools and recreational waters: a systematic review and meta-analysis. Parasitol Res 2022;121(11):3033–3050.
5. Gharpure R, Bliton J, Goodman A, *et al.* Epidemiology and clinical characteristics of primary amebic meningoencephalitis caused by *Naegleria fowleri*: a global review. Clin Infect Dis 2021;73(1):E19–27.
6. Siddiqui R, Khan NA. Primary amoebic meningoencephalitis caused by *Naegleria fowleri*: an old enemy presenting new challenges. PLoS Negl Trop Dis 2014;8(8):e3017.
7. Maciver SK, Piñero JE, Lorenzo-Morales J. Is *Naegleria fowleri* an emerging parasite? Trends Parasitol 2020;36(1):19–28.
8. Visvesvara GS, Moura H, Schuster FL. Pathogenic and opportunistic free-living amoebae: *Acanthamoeba spp*., *Balamuthia mandrillaris*, *Naegleria fowleri*, and *Sappinia diploidea*. FEMS Immunol Med Microbiol 2007;50(1):1–26.
9. Jahangeer M, Mahmood Z, Munir N, *et al. Naegleria fowleri*: sources of infection, pathophysiology, diagnosis, and management; a review. Clin Exp Pharmacol Physiol 2020;47(2):199–212.
10. Piñero JE, Chávez-Munguía B, Omaña-Molina M, *et al. Naegleria fowleri*. Trends Parasitol 2019;35(10):848–9.
11. Rajendran K, Ahmed U, Meunier AC, *et al.* Nanoparticle-terpene fusion: a game-changer in combating primary amoebic meningoencephalitis caused by *Naegleria fowleri*. ACS Omega 2024;9(10):11597–607.
12. Pugh JJ, Levy RA. *Naegleria fowleri*: diagnosis, pathophysiology of brain inflammation, and antimicrobial treatments. ACS Chem Neurosci 2016;7(9):1178–1179.
13. Ženíšková K, Mach J, Arbon D, *et al.* The 4-aminomethylphenoxy-benzoxaborole AN3057 as a potential treatment option for primary amoebic meningoencephalitis. Antimicrob Agents Chemother 2023;67(2).
14. Meunier AC, Nair R, Zher LY, *et al.* Recent advances in natural and nanoparticle-based therapies for *Naegleria fowleri* infections. Prog Microbes Mol Biol 2025;8(1).

15. Chao-Pellicer J, Arberas-Jiménez I, Fuchs F, *et al*. Repurposing of nitroxoline as an alternative primary amoebic meningoencephalitis treatment. Antibiotics. 2023 Aug 3;12(8):1280.
16. Arjmand F, Tabassum S, Khan HY. Molecular docking and computational in silico investigations of metal-based drug agents. Adv Prospects 3-d Metal-Based Anticancer Drug Candidates. 2024;149–168.
17. Salmaso V, Moro S. Bridging molecular docking to molecular dynamics in exploring ligand-protein recognition process: an overview. Front Pharmacol 2018;9.
18. Abdullahi M, Adeniji SE. In-silico molecular docking and ADME/pharmacokinetic prediction studies of some novel carboxamide derivatives as anti-tubercular agents. Chem Africa 2020;3(4):989–1000.
19. Cope JR, Ali IK. Primary amebic meningoencephalitis: what have we learned in the last five years? Curr Infect Dis Rep 2016;18(10):31.
20. Capewell LG, Harris AM, Yoder JS, *et al.* Diagnosis, clinical course, and treatment of primary amoebic meningoencephalitis in the United States, 1937–2013. J Pediatric Infect Dis Soc 2015;4(4):e68–75.
21. Oncel K, Karaagac L, Dagcı H, *et al.* Real-time PCR confirmation of a fatal case of primary amoebic meningoencephalitis in Turkey caused by *Naegleria fowleri*. Acta Parasitol 2022;67(2):697–704.
22. Visvesvara GS. Infections with free-living amebae. Handb Clin Neurol 2013;114:153–168.
23. Elsalami RM, Goh KW, Mahadi M, *et al.* The antibacterial activities of secondary metabolites derived from Streptomyces sp. Prog Microbes Mol Biol 2022;5(1).
24. Battah B, Rajab A, Shbibe L, *et al.* Evaluation of antibiofilm activity of *Thymus syriacus* essential oil against clinically isolated MDR bacteria. Prog Microbes Mol Biol 2022;5(1).
25. Chong YM, Yin WF, Ho CY, *et al.* Malabaricone C from Myristica cinnamomea exhibits anti-quorum sensing activity. J Nat Prod 2011;74(10):2261–2264.
26. Lim WQ, Cheam JY, Law JWF, *et al.* Role of garlic in chronic diseases: focusing on gut microbiota modulation. Prog Microbes Mol Biol 2022;5(1).
27. Cárdenas-Zúñiga R, Silva-Olivares A, Villalba-Magdaleno JDA, *et al.* Amphotericin B induces apoptosis-like programmed cell death in *Naegleria fowleri* and *Naegleria gruberi.* Microbiology 2017;163(7):940–9.
28. Grace E, Asbill S, Virga K. *Naegleria fowleri*: pathogenesis, diagnosis, and treatment options. Antimicrob Agents Chemother 2015;59(11):6677–6681.
29. Leong CF, Ming LC, Aroua MK, *et al.* Therapeutic and pharmacological role of natural products in neurological diseases: targeting autophagy pathways. Prog Microbes Mol Biol 2025;8(1).
30. Bellini NK, Santos TM, da Silva MTA, *et al.* The therapeutic strategies against *Naegleria fowleri*. Exp Parasitol 2018;187:1–11.
31. Rajendran K, Anwar A, Khan NA, *et al.* Oleic acid coated silver nanoparticles showed better *in vitro* amoebicidal effects against *Naegleria fowleri* than amphotericin B. ACS Chem Neurosci 2020;11(16):2431–7.
32. Othman MA, Sivasothy Y. Acylphenols and Dimeric Acylphenols from the Genus Myristica: A Review of Their Phytochemistry and Pharmacology. Plants. 2023 Apr 9;12(8):1589.
33. Mungroo MR, Anwar A, Khan NA, *et al.* Gold-conjugated curcumin as a novel therapeutic agent against brain-eating amoebae. ACS Omega 2020;5(21):12467–12475.
34. Liu Y, Yang X, Gan J, *et al.* CB-Dock2: improved protein–ligand blind docking by integrating cavity detection, docking and homologous template fitting. Nucleic Acids Res 2022;50(W1):W159–W164.

35. Yang X, Liu Y, Gan J, *et al.* FitDock: protein–ligand docking by template fitting. Brief Bioinform 2022;23(3).
36. Devaurs D, Antunes DA, Hall-Swan S, *et al.* Using parallelized incremental meta-docking can solve the conformational sampling issue when docking large ligands to proteins. BMC Mol Cell Biol 2019;20(1):42.
37. Páll S, Abraham MJ, Kutzner C, *et al.* Tackling exascale software challenges in molecular dynamics simulations with GROMACS. International conference on exascale applications and software 2015;3–27.
38. Abraham MJ, Murtola T, Schulz R, *et al.* GROMACS: high performance molecular simulations through multi-level parallelism from laptops to supercomputers. SoftwareX 2015;1–2:19–25.
39. Huang J, Rauscher S, Nawrocki G, *et al.* CHARMM36: an improved force field for folded and intrinsically disordered proteins. Biophys J 2017;112(3):175a–176a.
40. Vanommeslaeghe K, Raman EP, MacKerell AD. Automation of the CHARMM General Force Field (CGenFF) II: assignment of bonded parameters and partial atomic charges. J Chem Inf Model 2012;52(12):3155–3168.
41. Vanommeslaeghe K, MacKerell AD. Automation of the CHARMM General Force Field (CGenFF) I: bond perception and atom typing. J Chem Inf Model 2012;52(12):3144–3154.
42. Vanommeslaeghe K, Hatcher E, Acharya C, *et al.* CHARMM general force field: a force field for drug-like molecules compatible with the CHARMM all-atom additive biological force fields. J Comput Chem 2010;31(4):671–690.
43. Lemkul JA. Introductory tutorials for simulating protein dynamics with GROMACS. J Phys Chem B 2024;128(39):9418–9435.
44. Valdés-Tresanco MS, Valdés-Tresanco ME, Valiente PA, *et al.* gmx_MMPBSA: a new tool to perform end-state free energy calculations with GROMACS. J Chem Theory Comput 2021;17(10):6281–6291.
45. Miller BR, McGee TD, Swails JM, *et al.* MMPBSA.py: an efficient program for end-state free energy calculations. J Chem Theory Comput 2012;8(9):3314–3321.
46. Yang X, Liu Y, Gan J, *et al.* FitDock: protein-ligand docking by template fitting. Brief Bioinform 2022;23(3).
47. Daina A, Michielin O, Zoete V. SwissADME: a free web tool to evaluate pharmacokinetics, drug-likeness and medicinal chemistry friendliness of small molecules. Sci Rep 2017;7(1):42717.
48. Fu L, Shi S, Yi J, *et al.* ADMETlab 3.0: an updated comprehensive online ADMET prediction platform enhanced with broader coverage, improved performance, API functionality and decision support. Nucleic Acids Res 2024;52(W1):W422–W431.
49. Banerjee P, Eckert AO, Schrey AK, *et al.* ProTox-II: a webserver for the prediction of toxicity of chemicals. Nucleic Acids Res 2018;46(W1):W257–W263.
50. Banerjee P, Kemmler E, Dunkel M, *et al.* ProTox 3.0: a webserver for the prediction of toxicity of chemicals. Nucleic Acids Res 2024;52(W1):W513–W520.
51. Schyman P, Liu R, Desai V, *et al.* vNN web server for ADMET predictions. Front Pharmacol 2017;8(DEC).
52. Daina A, Zoete V. A BOILED-Egg to predict gastrointestinal absorption and brain penetration of small molecules. ChemMedChem 2016;11(11):1117–1121.

53. Daina A, Michielin O, Zoete V. iLOGP: a simple, robust, and efficient description of n-octanol/water partition coefficient for drug design using the GB/SA approach. J Chem Inf Model 2014;54(12):3284–3301.
54. Drwal MN, Banerjee P, Dunkel M, *et al*. ProTox: a web server for the in silico prediction of rodent oral toxicity. Nucleic acids research. 2014 Jul 1;42(W1):W53-W58.
55. Yang H, Sun L, Li W, *et al*. In silico prediction of chemical toxicity for drug design using machine learning methods and structural alerts. Frontiers in chemistry. 2018 Feb 20;6:30.
56. Arulanandam CD, Hwang JS, Rathinam AJ, *et al*. Evaluating different web applications to assess the toxicity of plasticizers. Scientific reports. 2022 Nov 16;12(1):19684.
57. Lv W, Zhang X, Zhang H, *et al.* Safety of nutmeg powder by oral exposure: toxicity prediction and in vivo evaluation. Food Chem Toxicol 2025;200:115364.
58. Rajendran K, Anwar A, Khan NA, *et al.* Brain-eating amoebae: silver nanoparticle conjugation enhanced efficacy of anti-amoebic drugs against *Naegleria fowleri*. ACS Chem Neurosci 2017;8(12):2626–2630.
59. Ithoi I, Ahmad AF, Nissapatorn V, *et al*. Detection of *Naegleria* species in environmental samples from Peninsular Malaysia. PLoS One 2011;6(9):e24327.
60. Gabriel S, Khan NA, Siddiqui R. Occurrence of free-living amoebae (*Acanthamoeba*, *Balamuthia*, *Naegleria*) in water samples in Peninsular Malaysia. J Water Health 2019;17(1):160–171.
61. Kundu K, Nayak SK. Total syntheses of malabaricones B and C via a cross-metathesis strategy. J Nat Prod 2017;80(6):1776–1782.
62. Sivadas N, Kaul G, Akhir A, *et al.* Naturally derived malabaricone B as a promising bactericidal candidate targeting multidrug-resistant *Staphylococcus aureus* also possess synergistic interactions with clinical antibiotics. Antibiotics 2023;12(10).
63. Bauri AK, Foro S, Lindner HJ, *et al.* Malabaricone A isolated from a methanol extract of *Myristica malabarica*. Acta Crystallogr E Struct Rep Online 2006;62(4).
64. Chelladurai PK, Ramalingam R, Prem C, *et al. Myristica malabarica*: a comprehensive review. J Pharmacogn Phytochem 2017;6(2):255–258.
65. Ahmed U, Sivasothy Y, Khan KM, *et al.* Malabaricones from the fruit of *Myristica cinnamomea King* as potential agents against *Acanthamoeba castellanii*. Acta Trop 2023;248.
66. Vimalkumar PS, Sivadas N, Murali VP, *et al.* Exploring apoptotic induction of malabaricone A in triple-negative breast cancer cells: an acylphenol phyto-entity isolated from the fruit rind of *Myristica malabarica Lam*. RSC Med Chem 2024;15(10):3558–3575.
67. Manna A, Saha P, Sarkar A, *et al.* Malabaricone-A induces a redox imbalance that mediates apoptosis in U937 cell line. PLoS One 2012;7(5):e36938.
68. Ser HL, Yin WF, Chan KG, *et al.* Antioxidant and cytotoxic potentials of *Streptomyces gilvigriseus* MUSC 26T isolated from mangrove soil in Malaysia. Prog Microbes Mol Biol 2018;1(1).
69. Gabriel S, Masomian M, Poh CL, *et al.* Anti-dengue activity of revaprazan hydrochloride: a repurposed drug candidate. Prog Microbes Mol Biol 2025;8(1).
70. Rajendran K, Ahmed U, Meunier AC, *et al.* Natural terpenes inhibit the cytopathogenicity of *Naegleria fowleri* causing primary amoebic meningoencephalitis in the human cell line model. ACS Chem Neurosci 2023;14(23):4105–4114.

71. Patwardhan RS, Kundu K, Purohit V, *et al.* Malabaricone C, a constituent of spice *Myristica malabarica*, exhibits anti-inflammatory effects via modulation of cellular redox. J Biosci 2023;48(2):1–14.
72. Banerjee D, Bauri AK, Guha RK, *et al.* Healing properties of malabaricone B and malabaricone C against indomethacin-induced gastric ulceration and mechanism of action. Eur J Pharmacol 2008;578(2–3):300–312.
73. Goo YT, Grigoriev V, Korzun T, *et al.* Blood-brain barrier-penetrating nanocarriers enable microglial-specific drug delivery in hypothalamic neuroinflammation. Adv Healthc Mater 2025;14(13).
74. Liu S, Jin X, Ge Y, *et al.* Advances in brain-targeted delivery strategies and natural product-mediated enhancement of blood–brain barrier permeability. J Nanobiotechnol 2025;23(1):382.
75. Khan MS, Mohapatra S, Gupta V, *et al.* Potential of lipid-based nanocarriers against two major barriers to drug delivery—skin and blood–brain barrier. Membranes 2023;13(3):343.
76. Liu WY, Yu Y, Zang J, *et al.* Menthol-modified quercetin liposomes with brain-targeting function for the treatment of senescent Alzheimer's disease. ACS Chem Neurosci 2024;15(11):2283–2295.
77. Yu S, Wang X, Lv L, *et al.* Borneol-modified PEGylated graphene oxide as a nanocarrier for brain-targeted delivery of ginsenoside Rg1 against depression. Int J Pharm 2023;643:123284.
78. Patro BS, Tyagi M, Saha J, *et al.* Comparative nuclease and anti-cancer properties of the naturally occurring malabaricones. Bioorg Med Chem 2010;18(19):7043–51.
79. Hargrove TY, Kim K, Correia Soeiro MN, *et al.* CYP51 structures and structure-based development of novel, pathogen-specific inhibitory scaffolds. Int J Parasitol Drugs Drug Resist 2012;2:178–186.
80. Sze Ong Y, Tan LTH, Sunway B, *et al.* Cancer, natural products and nanodrug delivery systems. Prog Microbes Mol Biol 2020;3(1).
81. Shi D, Chahal KK, Oto P, *et al.* Identification of four amoebicidal nontoxic compounds by a molecular docking screen of *Naegleria fowleri* sterol Δ8-Δ7-isomerase and phenotypic assays. ACS Infect Dis 2019;5(12):2029–2038.
82. Siddiqui R, Abouleish MY, Khamis M, *et al.* Dual targeting of function-structure for effective killing of pathogenic free-living amoebae. ACS Med Chem Lett 2021;12(5):672–676.
83. Herbst R, Ott C, Jacobs T, *et al.* Pore-forming polypeptides of the pathogenic protozoon *Naegleria fowleri*. J Biol Chem 2002;277(25):22353–22360.
84. Yasmin N, Manna A, Sarkar SD, *et al.* Effectiveness of malabaricone-A in P-glycoprotein over-expressing cancer cell lines. Int J Basic Clin Pharmacol 2019;8(5):1051–1058.
85. Basak M, Mahata T, Chakraborti S, *et al.* Malabaricone C attenuates nonsteroidal anti-inflammatory drug-induced gastric ulceration by decreasing oxidative/nitrative stress and inflammation and promoting angiogenic autohealing. Antioxid Redox Signal 2020;32(11):766–784.
86. Checker R, Sharma D, Sandur SK, *et al.* Anti-inflammatory effects of plumbagin are mediated by inhibition of NF-kappaB activation in lymphocytes. Int Immunopharmacol 2009;9(7–8):949–958.
87. Checker R, Sharma D, Sandur SK, *et al.* Plumbagin inhibits proliferative and inflammatory responses of T-cells independent of ROS generation but by modulating intracellular thiols. J Cell Biochem 2010;110(5):1082–1093.
88. Chiu J, Dawes IW. Redox control of cell proliferation. Trends Cell Biol 2012;22(11):592–601.